Conference on Modelling Fluid Flow (CMFF'22)
The 18th International Conference on Fluid Flow Technologies
Budapest, Hungary, August 30-September 2, 2022

Performance Investigation of a Savonius Wind Turbine with Unconventional Blade Designs Inspired by Sand Eels

Islam HASHEM*[12], Emeel KERIKOUS[12], Stefan HOERNER[1], Dominique THÉVENIN[1]

[1] Laboratory of Fluid Dynamics and Technical Flows, Otto von Guericke University Magdeburg, 39106 Magdeburg, Germany.
[2] Mechanical Power Engineering Department, Faculty of Engineering-Mattaria, Helwan University, 11718 Cairo, Egypt. *Corresponding Author. E-mail: islam.hashem@ovgu.de

ABSTRACT

Wind turbines allow us to harness the power of the wind and turn it into mechanical energy. When the wind blows, the rotor blades spin, capturing available energy from the wind. Out of many kinds of wind turbines, efforts have been made here to improve the performance of Savonius turbines. The main drawback of such a turbine is its low efficiency. In the present study, a Savonius rotor with unconventional blade designs inspired biologically by sand eels has been proposed; aiming to improve its performance in terms of the output power coefficient (C_P). Sand eels are small elongated sea fish and can frequently be found in shallow water. Two main geometrical parameters have been considered and normalized by the blade diameter (d); the maximum camber (f_{max}) and the maximum camber location ($X_{f_{max}}$); whereas the maximum thickness (t_{max}) is kept as 20% of the maximum camber value to resemble the shape of a sand eel. A total of 54 blade designs have been evaluated using 2D numerical simulations to determine the aerodynamic behaviour of the new bio-inspired design. By comparison between th erotor with semi-circular arc blades and that with sand eel-like blades ($f_{max}/d = 0.4$ and $X_{f_{max}}/d = 0.8$), a noticeable improvement in the performance (up to 8.3% at $\lambda = 0.8$) can be obtained in this manner.

Keywords: Bio-inspiration, CFD, performance, sand eels, Savonius rotor

NOMENCLATURE

C_P	$[-]$	Power coefficient
C_Q	$[-]$	Torque coefficient
f_{max}	$[m]$	Maximum camber
t_{max}	$[m]$	Maximum thickness
$X_{f_{max}}$	$[m]$	Maximum camber location
θ	$[°]$	Azimuth angle
λ	$[-]$	Tip speed ratio
Ω	$[1/s]$	Angular speed

1. INTRODUCTION

Due to the global energy crisis, research and development activities in the field of renewable energy, particularly wind energy, have increased significantly in many nations in recent years. Wind turbines are well-known devices for harvesting available energy from the wind and transform it into mechanical energy. Wind turbines are mainly classified into horizontal axis wind turbines (HAWTs) and vertical axis wind turbines (VAWTs). Horizontal axis wind turbines (HAWTs) are currently the most common type of wind turbines used for power generation. However, the performance of these turbines is limited due to the need for orientation mechanism (yaw), high installation cost, and the need for high-speed wind. Therefore, vertical axis wind turbines (VAWTs) have recently gained importance as a suitable alternative for energy production in residential and isolated places with low-speed wind. Vertical axis wind turbines (VAWTs) are divided into two basic types, Darrieus-type and Savonius-type rotors (Figure 1). The Darrieus-type VAWT was patented by the French engineer J. M. Darrieus in 1931 [1]. In principle, it consists of two curved blades with airfoil cross-section profile that generate aerodynamic lift, when the wind passes over its surface, as shown in Figure 1(a). The Savonius-type VAWT was invented by J. Savonius in 1929 [2]. The Savonius turbine is mainly a drag-driven VAWT and consists in its original design of two semi-circular buckets attached to a rotating shaft in opposing directions, as shown in Figure 1(b). Savonius wind turbines are commonly used owing to the simple design of its blades. Moreover, they are characterized by capability of self-starting, ability to capture wind from any direction, low manufacturing and maintenance costs, robustness and low cut-in speed. However, Savonius wind turbines have poor efficiency (less than 25%) compared to other types of wind turbines. Therefore, many researchers have tried to modify blade design and geometical parameters of the Savonius rotors,

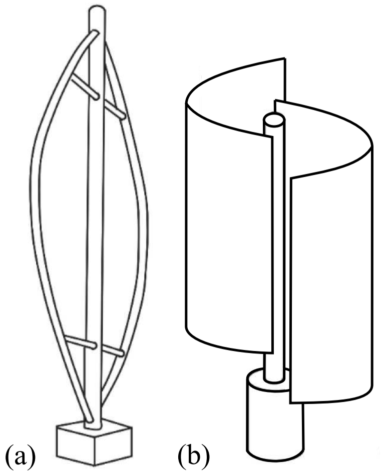

Figure 1. A schematic of vertical axis wind turbines (VAWTs): (a) Darrieus-type and (b) Savonius-type

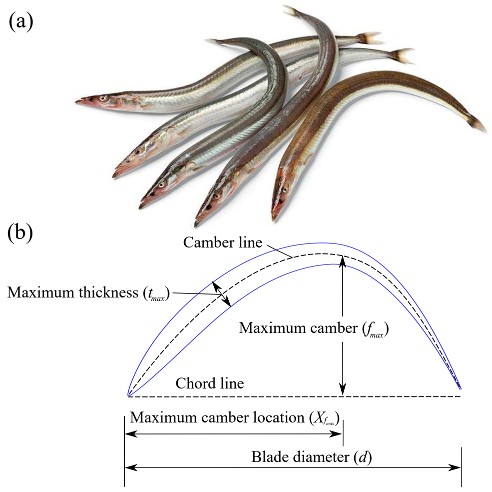

Figure 2. Analogy between sand eels (a) and bio-inspired blades (b) suggested for a Savonius rotor

aiming to increase its efficiency. Some important works from the literature about unconventional blade designs to improve the performance of Savonius rotors are reported in Table 1.

2. PURPOSE OF THE PRESENT STUDY

Sand eels, also known as sand lances, are small, slender eel-like fish that grow to be approximately 9 inches long and often live in vast shoals. An analogy between sand eels and bio-inspired blades suggested for Savonius wind turbines is shown in Figure 2. However, while keeping the general geometrical ratios analog to a sand-eel shape (Figure 2(a)) the particular geometry, such as curvature should be adjusted for improved aerodynamics. For this purpose, two main geometrical parameters of the sand-eel inspired blade (Figure 2(b)) have been considered and normalized by the blade diameter (d); the maximum camber (f_{max}) and the maximum camber location ($X_{f_{max}}$); whereas the maximum thickness (t_{max}) is kept as 20% of the maximum camber value to remain in geometric ratios of a sand eel. In this way, a total of 54 sand eel-like blades have been generated and investigated as Savonius wind turbine to increase the turbine performance, as depicted in Figure 3. This is the focus of the present study.

3. METHODOLOGY

Savonius rotors typically consist of two semi-circular arc blades, namely advancing blade (Blade A) and returning blade (Blade R). Figure 4 shows the geometrical parameters of a standard Savonius rotor as described by Hayashi et al. [12] in their experiment. D is the rotor diameter, H is the rotor height, S is the rotor overlap, d is the blade diameter and a is the shaft diameter. The azimuth angle (θ) is 0 when the chord line is parallel to the wind direction U_0. The length along the circular arc (l) is calculated as $\pi/2$. The coordinate s is defined along the circular arc so that s/l is 0 and 1 at leading edge and trailing edge, respectively. The specifications of the tested rotor and its main dimensions are listed in Table 2.

By referring to the notations of Figure 4, the tip speed ratio (λ) is defined as:

$$\lambda = \frac{\Omega D}{2U_0} \tag{1}$$

The mechanical torque Q and the mechanical power P output from the Savonius rotor can be defined in non-dimensional forms as:

$$C_Q = \frac{4Q}{\rho D^2 H U_0^2} \tag{2}$$

and

$$C_P = \frac{2P}{\rho D H U_0^3} \tag{3}$$

where C_Q and C_P are the torque power coefficient and power coefficient of the Savonius rotor, respectively. The corresponding values of C_Q and C_P at each tip speed ratio (λ) are used to characterize the global performance of the turbine.

In the present study, the geometry is treated in two dimensions since the blade section is simply extruded along the rotor height. However the 2D approach will neglect any 3D effects, such as those from presence of the end plates. The computational grids are generated with the trimmed cell mesher. The mesh consists of two grid components, namely, background and rotor meshes, in addition to the wake refinement that is embedded in the background mesh (see Figure 5). An overset mesh approach was applied in-between the background and the rotor meshes. The domain size is $-10D \times 30D$ in x-direction and $10D$ wide in y-direction to avoid any confinement effects. Figure 5(d) shows a typical mesh around the blade with 18 prism layers next to

Table 1. A review of unconventional blade designs from literature about Savonius rotors

Design	Description	Gain
Dual splitters [3]	Dual splitters are introduced to the concave side of a Savonius rotor through two approaches; top splitter fixed or bottom splitter fixed	A blade with top splitter positioned at 105° succeeded in improving the performance of the Savonius rotor by 7.3%
Koi fish-like blade [4]	Metamodeling-based optimization is applied to optimize the overlap ratio and gap ratio of a Savonius rotor with two blades inspired by a couple of swimming Koi fish	A Savonius rotor consists of two Koi fish-like blades with overlap and gap ratios of 0.2085 and 0.0057 exhibited about 17.6% increase in output power coefficient
V-shaped rotor [5]	A Savonius rotor of aspect ratio of 0.7 was developed by varying length and arc radius of 90° V-edges of the V-shaped blade profile	About 19.3% increase in the maximum power coefficient of a Savonius rotor having V-edge length and arc radius of 0.43 and 0.56 times the reference length, respectively
Thick blade [6]	An optimization process including 12 geometrical parameters was executed to obtain a thick (non-constant thickness) blade profile	A relative increase of 12% in output power coefficient has been reported at λ=1.1
Different concave and convex sides [7]	An optimization procedure was adopted to independently modify the convex and concave surface shapes of a classical Savonius rotor blade	The power coefficient was increased by about 4.41% through Particle Swarm Optimization (PSO) applied to optimize the concave and convex sides
Multiple quarter blades [8]	A new configuration comprises multiple quarter blades added to the traditional configuration of a Savonius rotor	An improvement in power coefficient ranging between 8.89% and 13.69% for different inlet velocities has been obtained by using multiple quarter blades
Combined blades [9]	A combination was made between semi-circular arc-shaped blade and concave elliptical-shaped blade to enhance the performance of a reference Savonius rotor.	An increase up to 11% in output power coefficient can be achieved through the application of combined blades
Airfoil-shaped blade [10]	A Savonius rotor comprises innovative airfoil-shaped blades was developed by modifying Goettingen 462 and NACA 0012 airfoils, resulting in SR3345 and SR5050 airfoils, respectively	The SR3345 achieved a slight increase in C_P at λ<0.5, while the SR5050 rotor showed an enhancement in performance at λ>0.9. However, both rotors exhibited lower C_P-values than that of the conventional rotor at 0.5<λ<1.0
Myring Equation-based blade [11]	A novel blade shape was designed according to Myring Equation with the aim of increasing the power coefficient of the conventional Savonius rotor	A Savonius rotor with a blade fullness of 1 resulted in 10.98% better performance than a conventional Savonius rotor

the wall. The averaged y^+ is kept less than unity to capture accurately the viscous boundary layer. A mesh independence test is carried out at the design tip speed ratio ($\lambda = 0.8$). The mesh density increased gradually from coarse to fine by a refinement ratio of about 1.3. Following three mesh refinements, a difference of less than 1% is obtained. The total number of cells employed is about 200k. The simulation requires about 24h to complete 20 revolutions on two parallel nodes of the HPC-Cluster at "Otto von Guericke" University Magdeburg.

The commercial software Simcenter STAR-CCM+ 2021.3 is used for the solution of the unsteady Reynolds-averaged Navier-Stokes (URANS) equations. The $k-\omega$ Shear-Stress-Transport (SST) turbulence model by Menter [13] was applied. This

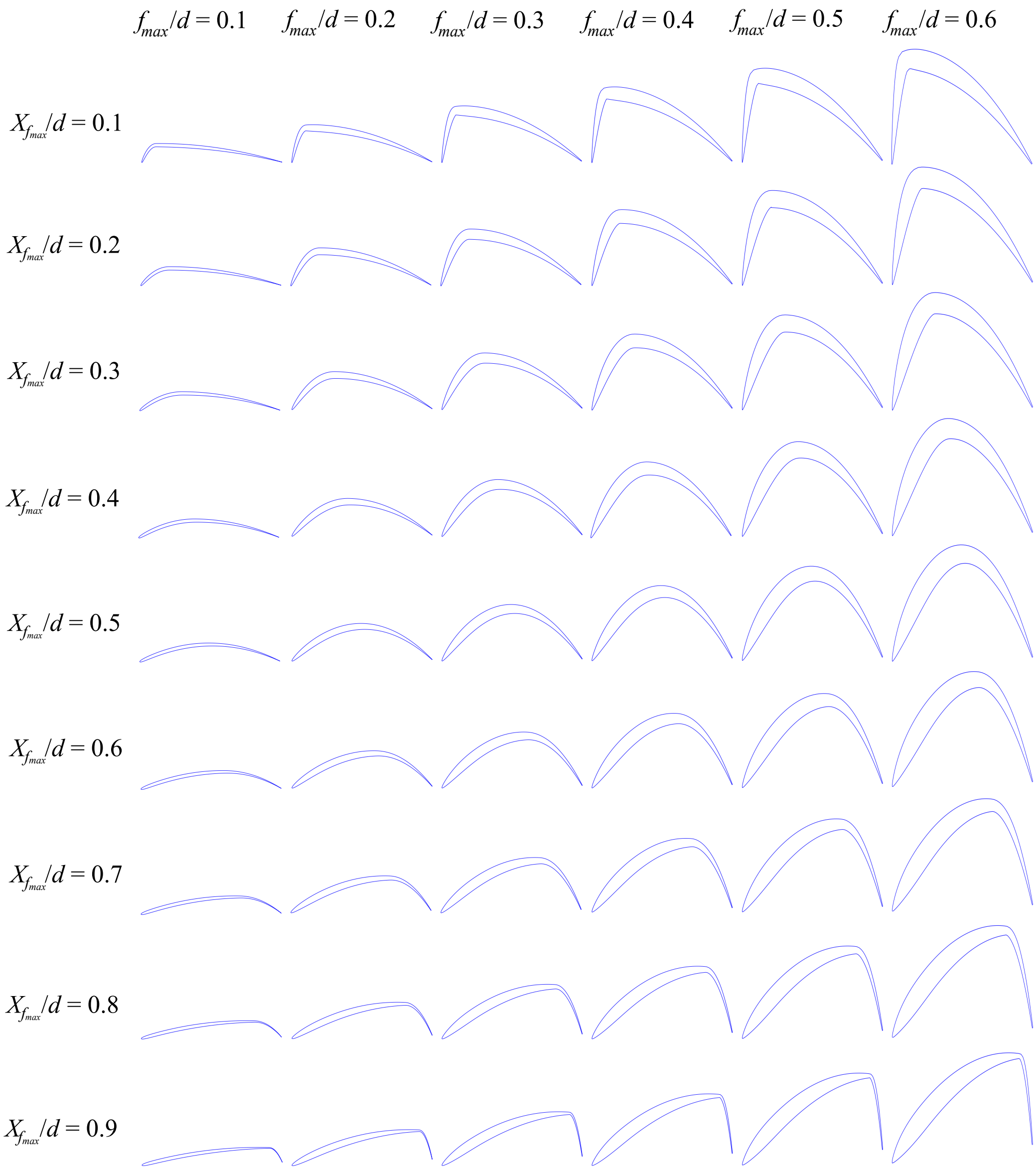

Figure 3. Various models of sand eel-like blades with different values of maximum camber (f_{max}) and maximum camber location ($X_{f_{max}}$) at t_{max} = 20% f_{max}

Table 2. Specifications of the Savonius rotor with semi-circular arc blades [12]

Parameter	Value
Rotor diamater D	0.33 m
Rotor height H	0.23 m
Rotor overlap C	0.066 m
Blade diamater d	0.184 m
Shaft diamater a	0.015 m

model delivers efficient predictions for flows involving strong adverse pressure gradients. Double-precision accuracy of floating point numbers and second-order discretization in space and time is applied. The governing equations are solved using a segregated flow solver. Three different timestep sizes corresponding to azimuth angles of 2°, 1° and 0.5° were investigated. According to the results of a time-independent analysis, a timestep size of 0.5° is found necessary for the present numerical simulations.

The number of revolutions plays a critical role in obtaining a converged solution for numerical simulations of turbomachinery. To maintain reasonable computational time, each numerical simulation was allowed to run for 20 revolutions to ensure that the average torque coefficient (C_Q) shows periodicity in time. After 20 revolutions (t = 4.32 s), the average

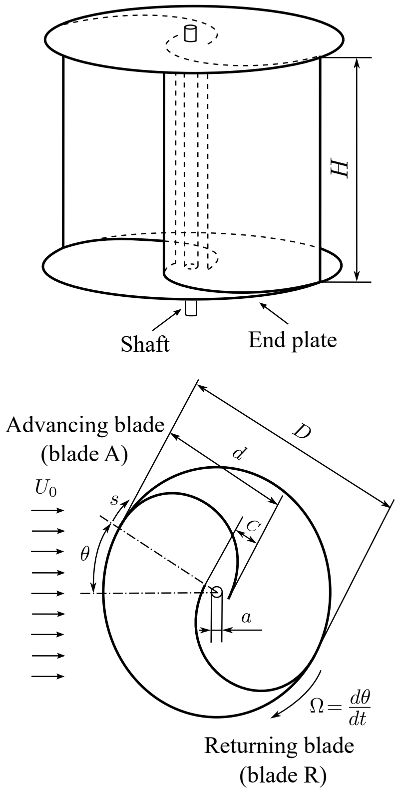

Figure 4. Geometry of the standard Savonius rotor

torque coefficient (C_Q) does not show any significant changes over time (variations below 0.003). The average torque coefficient (C_Q) has always been calculated by time-averaging the values over the last five revolutions.

4. RESULTS AND DISCUSSION

The full numerical procedure has been validated with published numerical results [14] and experimental measurements [12] based on a standard Savonius rotor. The present numerical results match very well with numerical results of Mohamed et al. (2011), both using the $k-\omega$ SST turbulence model (see Figure 6). However, there is a significant deviation compared to the experimental measurements that can be attributed to the 2D assumption. It is worth mentioning that the presence of endplates in the experiment conducted by Hayashi et al. [12] is not taken into account in the present study.

As can be noticed from Figure 6(b), the maximum deviation between the present numerical 2D results and experimental measurements for C_P is about 37.30%. A comparable deviation has been reported by Mohamed et al. [14] and Hosseini Imeni et al. [15] as 36.45% and 25.44%, respectively; all these studies involve 2D numerical simulations with the $k-\omega$ SST model. In other words, the $k-\omega$ SST model usually overpredicts the performance of Savonius rotors when the problem is modeled as two-dimensional or planar. To support this statement, the maximum deviation between the numerical results and experimental measurements is reduced to be only 12.22% when a 3D numerical simulation is carried out, as reported by Elmekawy et al. [16].

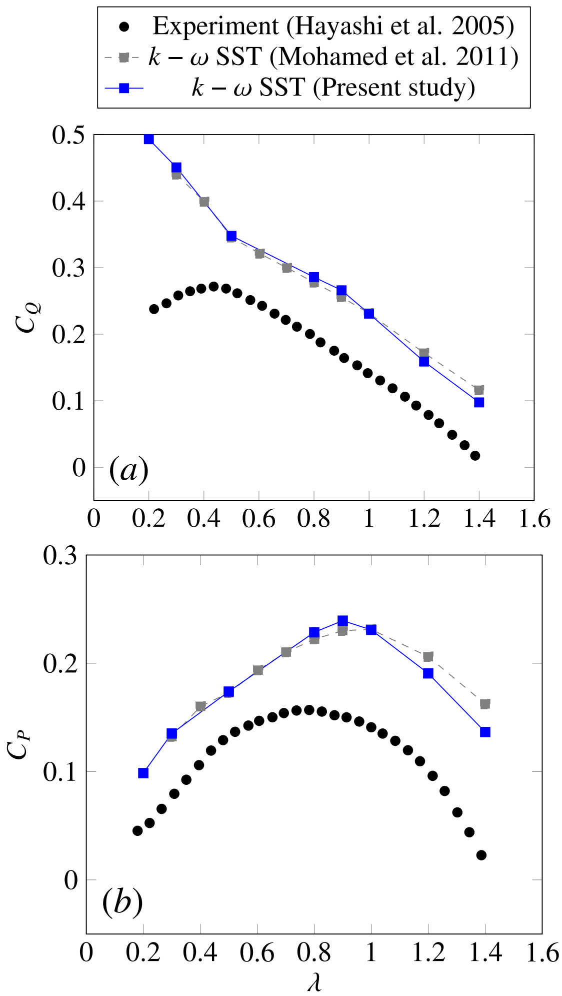

Figure 6. A comparison of the predicted (a) torque coefficient (C_Q) and (b) power coefficient (C_P) to published numerical results [14] and experimental measurements [12]

Before starting the parametric study, two different arrangements of sand eel-like blades were examined at the design tip speed ratio ($\lambda = 0.8$), one when the fish head is facing outward and the other when the fish head is facing inward with respect to the rotor axis. This preliminary study showed that the output power coefficient (C_P) is higher when the fish head is facing inward compared to the other arrangement. Therefore, only one arrangement (fish head facing inward) is considered in the parametric study (see Figure 5).

Figure 7 represents a scatter plot for the calculated power coefficient (C_P) of sand eel-like blades with different maximum camber (f_{max}/d) and maximum camber location ($X_{f_{max}}/d$) values at $\lambda = 0.8$. The highest performance could be achieved with

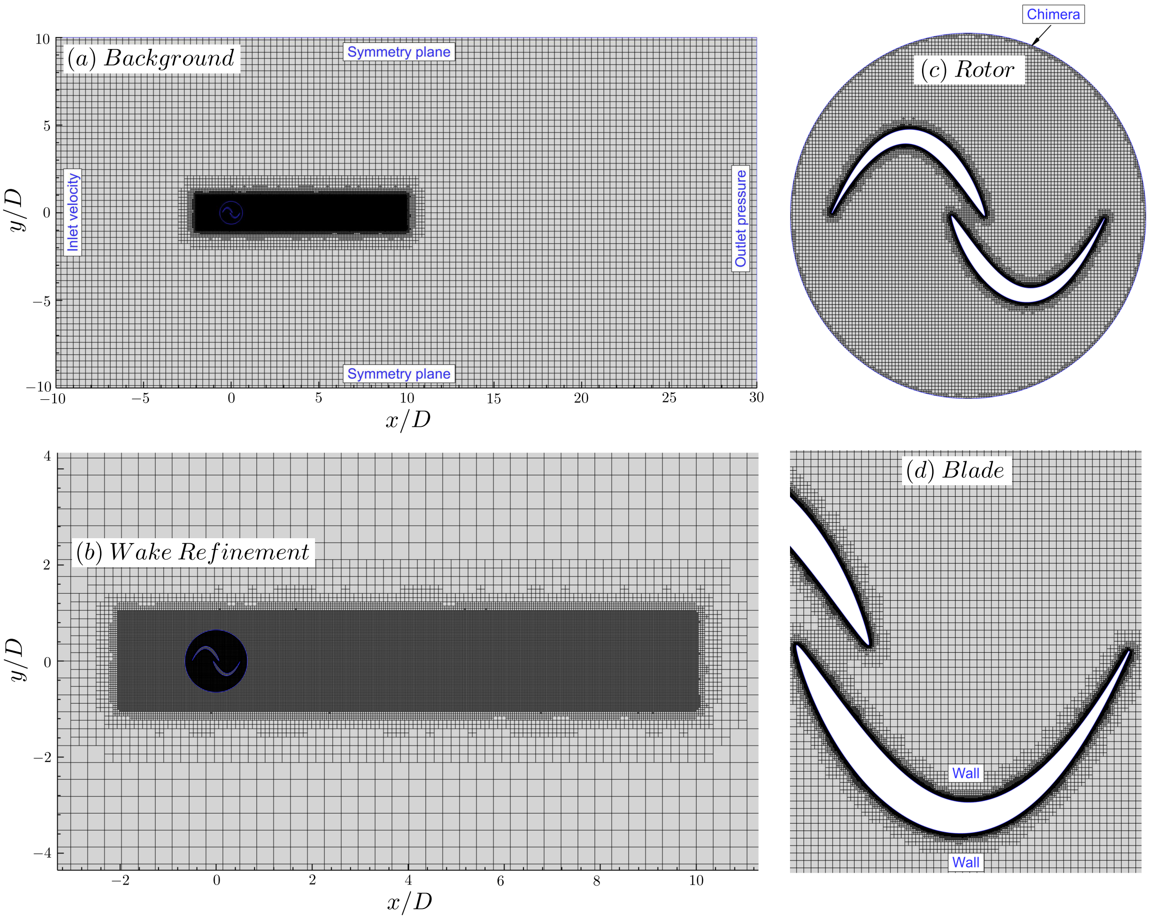

Figure 5. Computational mesh for a Savonius rotor with sand eel-like blades: background (a), wake refinement (b), rotor (c) and blade (d). The boundary conditions are described by the blue-coloured text

high cambered sand-eel like blades, particularly at camber locations ($X_{f_{max}}/d$) of 0.5 and 0.8. On the other hand, sand eel-like blades with low camber and camber location values deliver the worst performance for the Savonius wind turbine. From the simulations, the output power coefficient (C_P) has been calculated for 54 sand eel-like blades. In this manner, the best and the worst blade designs could thus easily be distinguished for $\lambda = 0.8$. Therefore, the best blade design corresponds to $f_{max}/d = 0.4$ and $X_{f_{max}}/d = 0.8$ with $C_P = 0.2486$ whereas a blade design with $f_{max}/d= 0.1$ and $X_{f_{max}}/d= 0.1$ exhibited the lowest power coefficient ($C_P = 0.0581$), as presented in Figure 7. For the best-performing sand eel-like blade ($f_{max}/d = 0.4$ and $X_{f_{max}}/d = 0.8$), this gain leads to an improvement in turbine performance of about 8.3% at the design tip speed ratio ($\lambda = 0.8$), compared to a Savonius wind turbine with semi-circular arc blades.

Figure 8 shows the streamlines around the standard Savonius wind turbine with semi-circular arc blades (a) and that with the best-performing sand eel-like blades (b) at $\lambda = 0.8$. For both rotors, a separation vortex can be observed on the convex side located near the leading edge (fish head) of the advancing blade (blade A). However, the separation vortex is less intensive for the sand eel-like blade. It can be noticed that the stagnation point on the surface of the returning blade (blade R) of the sand eel-like blade is shifted to occur near the trailing edge (fish tail) whereas it occurs nearly at middle of the semi-circular arc blade. The flow through the gap between the blades is more pronounced in case of the Savonius rotor with sand eel-like blade compared to the standard rotor.

The pressure distributions at $\lambda = 0.8$ are shown in Figure 9. The deep differences in the pressure distributions between the two rotors due to different blade designs are obvious. The sand eel profile experiences considerably higher pressure on the concave surface of the advancing blade (blade A) compared to the semi-circular arc. Moreover, the pressure is relatively lower on the convex side of the sand eel-like blade than for the semi-circular blade. The larger pressure difference between both sides of the sand eel-like blades produces a higher force, explaining the better performance.

5. CONCLUSIONS

The present study investigated the performance of a Savonius wind turbine with unconventional

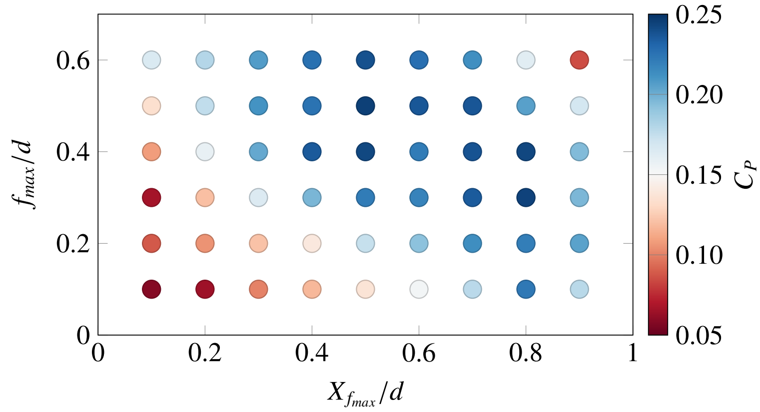

Figure 7. Scatter plot for different maximum camber (f_{max}/d) and maximum camber location ($X_{f_{max}}/d$) values colored by power coefficient (C_P) of the Savonius rotor with sand eel-like blades at λ = 0.8

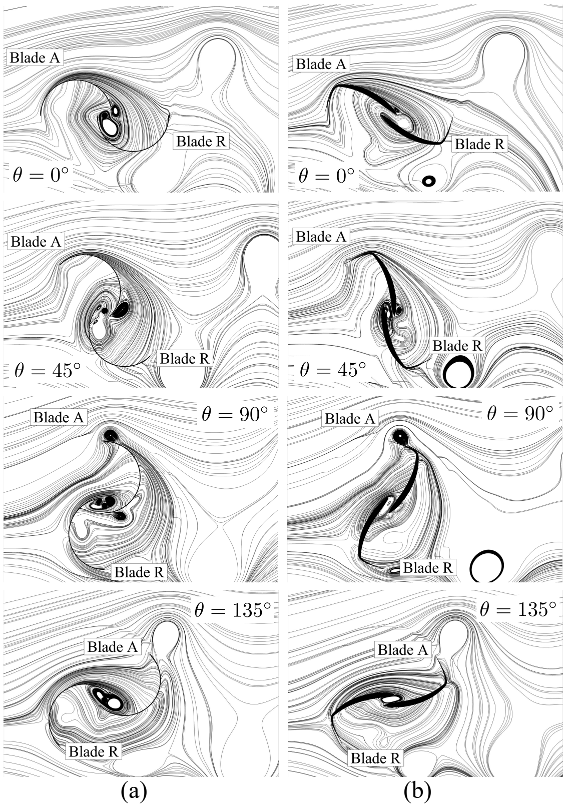

Figure 8. Streamlines around Savonius rotor with semi-circular arc blades (a) and that with the best-performing sand eel-like blades (b) at λ = 0.8

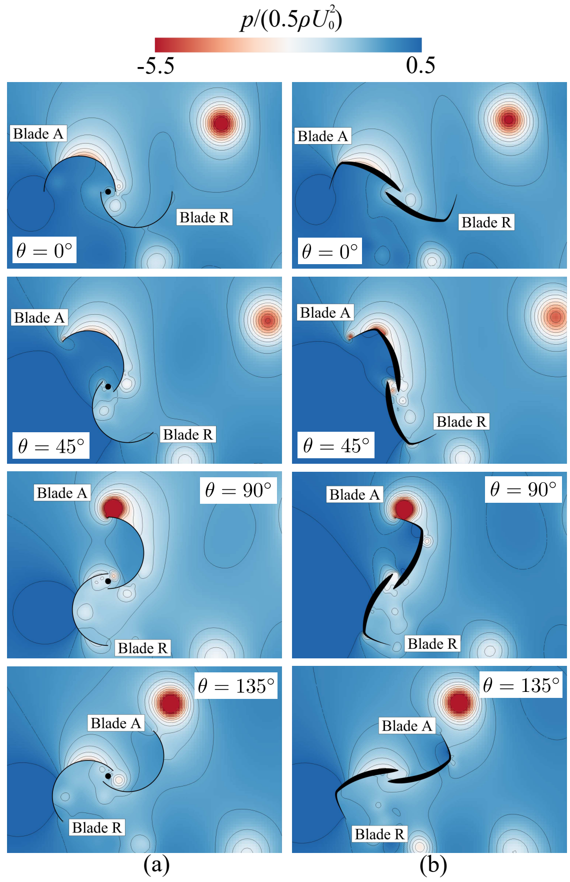

Figure 9. Pressure distributions of Savonius rotor with semi-circular arc blades (a) and that with the best-performing sand eel-like blades (b) at λ = 0.8

blade designs inspired biologically by sand eels. A total of 54 sand eel-like blades are obtained by changing the camber and camber location of bio-inspired blades that fitted into a Savonius rotor. The new bio-inspired blade designs were evaluated by means of 2D numerical simulations to assess the performance in terms of output power coefficient (C_P). The parametric study identifies a better Savonius rotor than the standard one with semi-circular blades, leading to an improvement in performance by 8.3% at the design tip speed ratio (λ = 0.8). Analyzing the flow field around both Savonius rotors explains this superior performance.

In this study, the best-performing bio-inspired blade has been obtained manually out of 54 designs.

It might not be the optimal one. Accordingly, the next step could involve a systematic optimization procedure to reach the optimal sand eel-like blade. Furthermore, in the present parametric study, the sand eel-like blades were evaluated only at the design tip speed ratio (λ = 0.8). However, the new blade should also be tested at off-design conditions (several λ-values) to check how the gain changes through the full operating range.

ACKNOWLEDGEMENTS

The first author would like to thank Prof. Dr.-Ing. habil. Gábor Janiga for his continued support.

REFERENCES

[1] Marie, D. G. J., 1931, "Turbine having its rotating shaft transverse to the flow of the current", US Patent 1,835,018.

[2] Johannes, S. S., 1929, "Rotor adapted to be driven by wind or flowing water", US Patent 1,697,574.

[3] Patel, V., and Patel, R., 2021, "Free energy-extraction using Savonius hydrokinetic rotor with dual splitters", *Materials Today: Proceedings*, Vol. 45, pp. 5354–5361.

[4] Hashem, I., and Zhu, B., 2021, "Metamodeling-based parametric optimization of a bio-inspired Savonius-type hydrokinetic turbine", *Renewable Energy*, Vol. 180, pp. 560–576.

[5] Shashikumar, C., Honnasiddaiah, R., Hindasageri, V., and Madav, V., 2021, "Experimental and numerical investigation of novel V-shaped rotor for hydropower utilization", *Ocean Engineering*, Vol. 224, p. 108689.

[6] Kerikous, E., and Thévenin, D., 2019, "Optimal shape of thick blades for a hydraulic Savonius turbine", *Renewable energy*, Vol. 134, pp. 629–638.

[7] Tian, W., Mao, Z., Zhang, B., and Li, Y., 2018, "Shape optimization of a Savonius wind rotor with different convex and concave sides", *Renewable energy*, Vol. 117, pp. 287–299.

[8] Sharma, S., and Sharma, R. K., 2016, "Performance improvement of Savonius rotor using multiple quarter blades–A CFD investigation", *Energy Conversion and Management*, Vol. 127, pp. 43–54.

[9] Sanusi, A., Soeparman, S., Wahyudi, S., and Yuliati, L., 2016, "Experimental study of combined blade savonius wind turbine", *International Journal of Renewable Energy Research (IJRER)*, Vol. 6 (2), pp. 614–619.

[10] Tartuferi, M., D'Alessandro, V., Montelpare, S., and Ricci, R., 2015, "Enhancement of Savonius wind rotor aerodynamic performance: a computational study of new blade shapes and curtain systems", *Energy*, Vol. 79, pp. 371–384.

[11] Tian, W., Song, B., VanZwieten, J. H., and Pyakurel, P., 2015, "Computational fluid dynamics prediction of a modified Savonius wind turbine with novel blade shapes", *Energies*, Vol. 8 (8), pp. 7915–7929.

[12] Hayashi, T., Li, Y., and Hara, Y., 2005, "Wind tunnel tests on a different phase three-stage Savonius rotor", *JSME International Journal Series B Fluids and Thermal Engineering*, Vol. 48 (1), pp. 9–16.

[13] Menter, F. R., 1994, "Two-equation eddy-viscosity turbulence models for engineering applications", *AIAA journal*, Vol. 32 (8), pp. 1598–1605.

[14] Mohamed, M., Janiga, G., Pap, E., and Thévenin, D., 2011, "Optimal blade shape of a modified Savonius turbine using an obstacle shielding the returning blade", *Energy Conversion and Management*, Vol. 52 (1), pp. 236–242.

[15] Hosseini Imeni, S. Z., Kaabinejadian, A., Ami Ahmadi, H., and Moghimi, M., 2022, "Optimal design and sensitivity analysis of airfoil-shaped rotor blade for Savonius wind turbine by using response surface methodology", *Wind Engineering*, p. 0309524X211072868.

[16] Elmekawy, A. M. N., Saeed, H. A. H., and Kassab, S. Z., 2021, "Performance enhancement of Savonius wind turbine by blade shape and twisted angle modifications", *Proceedings of the Institution of Mechanical Engineers, Part A: Journal of Power and Energy*, Vol. 235 (6), pp. 1487–1500.